Functional characterization of a missense mutation in the V2 vasopressin receptor gene, *AVPR2*, causing a nephrogenic syndrome of inappropriate diuresis

László Sándor Erdélyi[1,2*], W. Alexander Mann[3*], Deborah J. Morris-Rosendahl[4], Ute Groß[5], Mato Nagel[6], Péter Várnai[1,2,] András Balla[1,2], László Hunyady[1,2]

[1] Department of Physiology, Semmelweis University, Faculty of Medicine, Budapest, Hungary

[2] MTA-SE Laboratory of Molecular Physiology, Hungarian Academy of Sciences and Semmelweis University, Budapest, Hungary

[3] Endokrinologikum Frankfurt a. Main, 60596 Frankfurt, Germany

[4]Genomic Medicine, National Heart and Lung Institute, Imperial College London, United Kingdom

[5] Molecular Diagnostics, Genteq GmbH, Hamburg, Germany

[6]Center for Nephrology and Metabolism, Weißwasser, Germany

*equally contributing authors

Correspondence author: László Hunyady

PO Box 259, H-1444 Budapest, Hungary, hunyady.laszlo@med.semmelweis-univ.hu

Short title: NSIAD caused by I130N mutation

Key words: type 2 vasopressin receptor, BRET, *AVPR2* gene, NSIAD

Word count (text): 3520

The authors declare that there is no conflict of interest that could be perceived as prejudicing the impartiality of the research reported.

This work was supported by Hungarian Ministry of National Resources (grant OTKA 100883).

Abstract

Nephrogenic syndrome of inappropriate diuresis is a recently-discovered rare disease caused by gain-of-function mutations of the V2 vasopressin receptor gene, *AVPR2*. To date, mutations of Phe229 and Arg137 have been identified as gain-of-function mutations in V2 vasopressin receptor (V2R). The mutant receptors lead to hyponatremia, which may lead to clinical symptoms in infants. In this study, we present a newly-identified Ile130Asn (I130N) substitution, causing NSIAD in a family. Characterization of the mutation revealed basal constitutive activity of V2R. We have demonstrated that the I130N mutation results in constitutive cAMP generation in HEK293 cells. Basal activity of the mutant receptor could be blocked by the inverse agonist tolvaptan and arginine-vasopressin stimulation enhanced the cAMP production of I130N-V2R. The mutation causes a biased receptor conformation since the basal cAMP generation activity of I130N does not lead to interaction with β-arrestin. The constitutive activity of the mutant receptor causes constitutive dynamin-dependent and β-arrestin-independent internalization. The inhibition of the basal internalization using dominant-negative dynamin resulted in an increased cell surface expression. In contrast to the constitutive internalization, agonist-induced endocytosis was β-arrestin dependent. Based on our findings, tolvaptan could be used for treatment of hyponatremia, shown in patients with nephrogenic syndrome of inappropriate diuresis who carry the I130N-V2R mutation.

Introduction

Mutations in G protein-coupled receptors (GPCR) may lead to broad spectrum of human diseases (1). The recently discovered nephrogenic syndrome of inappropriate antidiuresis (NSIAD) is caused by gain-of-function mutations in the *AVPR2* gene affecting the V2R (2). V2R is expressed in the plasma membrane of the principal cells in the kidney and mediates

the effect of the water homeostasis regulator arginine-vasopressin (AVP) through G_s-dependent cAMP production via adenylyl cyclase activation. Binding of AVP to the V2R leads to cAMP-mediated translocation of aquaporin-2 to the apical plasma membrane. This regulation of aquaporin-2 water channel localization is crucial for increasing urine osmolality and reducing urine output in humans (3). For precise regulation, the signal transduction of the activated GPCR has to be terminated to limit the effect in the target cells (4). Impairment of these processes may result in receptor dysfunction and disease, such as nephrogenic diabetes insipidus (NDI) in case of V2R (5).

Although more than 200 loss-of-function mutations affecting V2R have been identified (6), fewer NSIAD-causing gain-of-function mutations have been described. The first mutations were identified in infants who suffered from irritability and generalized seizures, resulting in substitutions of Arg137 to either Cys or Leu in the V2R (R137C or R137L) (2). The mutations caused elevated basal cAMP production in cells expressing the mutant receptors. Basal activity of R137C and R137L mutant V2Rs had similar properties to the NDI-causing R137H missense mutation, since the conformation of the mutant receptors also induced agonist-independent β-arrestin2 interaction (5, 7). Characterization of the R137C/L mutants revealed that although AVP stimulation caused increased β-arrestin binding, the agonist-induced cAMP generation was negligible, despite the affinity of the mutants toward AVP being unchanged (8). The data of Rochdi et al. may explain the clinical finding, that both the R137C and R137L mutations were insensitive to acute inverse agonist tolvaptan treatment (9, 10). Recently, a new NSIAD-causing substitution (F229V) in the V2R was found (11). Although F229V mutation was shown to have increased basal cAMP production, F229V-V2R had no detectible constitutive β-arrestin binding. F229V-V2R has a different constitutive active conformation from R137C/L receptors, since the cAMP generation could be further increased upon AVP stimulation. Moreover, the basal activity

could be blocked with inverse agonists. Another putative NSIAD mutation, V266A, has been reported, but it is considered to be a neutral polymorphism (12, 13). The patients with NSIAD at greatest risk are neonates and infants, who are vulnerable to hyponatremia and the consequent seizures (10, 14, 15). Therefore, a proposed therapeutic strategy based on functional studies of the mutant V2Rs could help these patients to minimize possible dangers of this genetic condition.

Here, we present a novel gain-of-function mutation of the V2R, identified in a patient and his family with hyponatremia. Functional studies were carried out to characterize the properties of the I130N-V2R. We demonstrate that the cellular effects of this mutation are different from those of previously described NSIAD-causing mutations. Based on our functional findings, a therapeutic recommendation could be proposed for patients carrying the I130N mutation.

Results

Identification of the I130N mutation in the *AVPR2* gene

The index patient was a 34-year old male with a long history of hyponatremia. Low sodium levels were first diagnosed at age 28 as part of a routine examination. Infancy and childhood of the patient was unremarkable. Except for occasional palpitations the patient was free of complaints. Further medical history included a tonsillectomy, pollen allergy, but not cerebral trauma or neuropsychological abnormalities. Medication at time of presentation was Nebivolol 2.5 mg/day, which was started at age 31 due to palpitations. No abnormal physical findings were noted; especially no edema or changes of skin color were detected. The average estimated fluid intake was 2-3 liters per day. Laboratory findings are shown in Table 1. AVP levels were low; sodium excretion in 24 h urine was elevated in an euvolemic state. The patient had marked hyponatremia in combination with low AVP levels compatible with

the diagnosis NSIAD, however this diagnostic entity is still under discussion (2). We studied the family of the index patient (Fig. 1). Two family members had low sodium levels: the mother and grandmother of the index patient, whereas father and sister had normal sodium levels (Table 2), consistent with an X-linked inheritance pattern of the disorder. All family members were in good general health, apart from degenerative joint and back complaints (I.2). Since the data confirmed the familial hyponatremia, we performed a molecular mutation analysis of the vasopressin type-2 receptor gene (AVPR2). Mutation analysis by direct DNA sequencing of PCR fragments from the proband and his family revealed a novel missense mutation, c.389T>A in exon 2 of the AVPR2 gene, which results in the amino acid change p.Ile130Asn. The proband was hemizygous for the mutation, whereas his mother (II.2), his sister (III.2) and his grandmother (I.2) were heterozygous for the p.Ile130Asn mutation confirming their carrier status. His father (II.1) showed a wild type sequence of the AVPR2 gene. The mutation was predicted by the Mutation Taster software to be "disease-causing" (probability score 0.999) and has not been previously recorded neither in the dbSNP database (www.ncbi.nlm.nih.gov/SNP/) nor in the NHLBI Exome Variant Server Database (http://evs.gs.washington.edu/EVS/).

Determination of cellular localization of the I130N-V2R

Confocal microscopy was implemented in order to determine the cellular localization of the I130N-V2R. The plasma membrane marker containing consensus sequence for myristoylation and palmitoylation (MP-Cerulean), the nuclear localization signal (NLS-mRFP) and either the WT-V2R or the I130N-V2R tagged with mVenus were transiently expressed in HEK293 cells (Fig. 2A). The mutant receptor showed similar intracellular fluorescence to the wild type receptor but the plasma membrane localization was less pronounced. For the conformation of the plasma membrane expression of the mutant receptor immunostaining with anti-HA-Alexa488 was performed in non-permeabilized cells co-

expressing NLS-mRFP and either HA-WT-V2R or HA-I130N-V2R (Fig. 2B). Confocal imaging clearly showed plasma membrane localization of the mutant receptor.

Investigation of the cAMP production of the I130N-V2R

For functional characterization, we monitored the cAMP production using BRET technique. Loading the Epac domain with cAMP causes conformational changes that move away the energy acceptor from the donor. Consequently, an increase in intracellular cAMP level results in a decreased BRET ratio in our measurements. As described previously, an increased cAMP concentration resulted in a decreased BRET ratio using the Epac-BRET sensor (16). Real-time monitoring of the cAMP levels were performed in living HEK293 cells expressing one of the following receptors: wild type receptor, I130N-V2R or N321K mutant receptor (this loss-of-function mutation has been characterized previously, reflecting the absence of basal activity) (16). The cells were treated first with tolvaptan, then with AVP (Fig. 3A-B). The basal BRET ratios were different for the various receptors, reflecting diverse basal cAMP levels. Wild-type (rectangle) showed known basal activity (16, 17). The basal BRET ratio of the I130N-V2R was markedly decreased, indicating constitutive activity of this mutant receptor (circle). Treatment of the wild-type and I130N receptor with the inverse agonist resulted in a decreased cAMP concentration (filled marks). Wild-type and I130N receptor stimulation with AVP resulted in a robust cAMP response (similar to forskolin treatment, Suppl. 2) and the kinetics of the cAMP response was similar. Fig. 3B shows the average of BRET ratios before and after stimulation. The dose-response curve of tolvaptan effect on the basal receptor activity was also determined. The inverse agonist tolvaptan had larger efficacy in case of the I130N-V2R mutant compared to the wild type receptor and potency was also determined (pEC_{50}:-7.94 ± 0.07 M for I130N-V2R, -8.15 ± 0.03 M forWT-V2R (Fig. 3C)).

Characterization of the plasma membrane expression of the I130N-V2R

Since constitutive activity could affect the presence of the receptor in the plasma membrane, we examined internalization properties. We performed flow cytometry measurements in order to assess the receptor quantity in plasma membrane of the cells. The relative fluorescent intensity (RFI) of the I130N mutant receptor (RFI: 0.59±0.1) was significantly lower than the RFI of the wild type receptor (RFI: 1.0) indicating decreased plasma membrane presence (Fig. 4A, n=4, $p<0.05$). We performed BRET measurements to monitor the change in receptor density in the plasma membrane. Cells were transfected with either WT-V2R or I130N-V2R tagged with Sluc bioluminescent donor (*Renilla* luciferase) and YFP-tagged plasma membrane marker containing consensus sequence for myristoylation and palmitoylation (MP-YFP). The non-specific energy transfer (BRET ratio) depends on the distance between the bioluminescent donor (receptor) and fluorescent acceptor (plasma membrane). Consequently, the decreased the BRET ratio reflects the altered localization of the energy donor and the acceptor, indicating the internalization of the cell surface localized receptors (16, 18, 19). Reflecting the flow cytometry data, there is remarkable difference between the basal BRET ratio of the wild type (Fig 4B, rectangle) and I130N receptor (circles), indicating a decreased plasma membrane presence of the mutant. Since the Sluc counts depend on the expression of the Sluc enzyme in the presence of the cell permeable substrate coelenterazine, the comparison of the normalized Sluc counts reflect the total protein level of the tagged receptors. The Sluc counts of WT-V2R and I130N-V2R were similar in the BRET measurements after the addition of cell permeable substrate reflecting that there was no significant difference in the level of the fused proteins (Suppl. 2). Tolvaptan could evoke a significant increase in the BRET ratio of the I130N-V2R. Next, we examined the agonist induced internalization of the receptor. Fig. 4C shows a robust fall in the BRET

ratios in the cells expressing the WT-V2R and the I130N mutant receptor in response to AVP treatment (filled marks).

Examination of the β-arrestin2 binding

We investigated the properties of the constitutive internalization of the I130N-V2R in detail. We compared the basal and agonist dependent β-arrestin2 binding of the wild-type and I130N mutant receptor with BRET technique. There was no difference in the basal BRET ratios (Fig. 5), which indicates the lack of β-arrestin2 binding of the constitutive active receptor. In accordance with that, tolvaptan treatment did not alter basal β-arrestin2 binding (data not shown). AVP stimulation yielded an increase in the BRET ratio between β-arrestin2 and the I130N-V2R, which was reduced than of WT-V2R (Fig. 5A).

Investigation of the internalization properties

We investigated the effect of dominant-negative dynamins in order to characterize the internalization properties of the I130N-V2R (8, 11). The wild-type dynamin1 could be used as a control, since there was no difference between the cotransfection of empty pcDNA3.1 or dynamin1 (Suppl. 3). Cells expressing the dominant-negative dynamin1 (Fig. 5B, DNdyn1-square) show an increased BRET ratio between the I130N-V2R-Sluc and the plasma membrane marker MP-YFP, compared to the effect of wild-type dynamin1 (dyn1, circle). Tolvaptan treatment could increase the plasma membrane presence of I130N-V2R-Sluc in the dominant-negative dynamin1 expressing cells (Fig 5B, filled rectangle), however this elevation was less than that of wild type dynamin1 expressing cells (filled circle).

Discussion

In this study, we present a novel gain-of-function mutation of the V2R, which we identified in a NSIAD patient with hyponatremia and low AVP levels. Sequencing of the *AVPR2* gene

revealed a missense mutation causing the amino acid substitution, p.Ile130Asn in the receptor (I130N-V2R). Characterization of the I130N-V2R revealed high basal concentration of cAMP in the cells expressing the mutant receptor (Fig. 3A-B). This constitutive activity of the mutant receptor could be blocked with the inverse agonist tolvaptan. This property of the I130N-V2R was similar to the consequence of the reported F229V mutation (11). Importantly, the treatment with tolvaptan instantly reduced the basal cAMP production of the receptor, which may raise the possibility of using tolvaptan in the therapy of NSIAD patients with I130N and similar mutations. In contrast to the R137C/L mutants, I130N-V2R showed increased cAMP production upon AVP stimulus (Fig 3A-B, (8)). Fig. 5A demonstrates that the I130N-V2R is capable of agonist-induced β-arrestin2 binding, while the constitutively active conformation, in spite of robust basal cAMP production, did not provoke detectible basal β-arrestin2 binding. Taken together, the constitutive active conformation of I130N-V2R in the absence of AVP differs from the agonist-induced active conformation of the receptor and clearly differs from the AVP-induced conformation of the wild-type receptor. In this regard, the I130N-V2R is similar to the F229V-V2R, since both share the characteristic property of the lack of basal β-arrestin2 binding, but not to R137C and R137L (7, 8, 11). These findings indicate that the I130N missense mutation can be considered as a biased mutant V2R, since the G-protein dependent pathway can be selectively activated. This phenomenon fit in the concept that GPCRs may have multiple active conformations with altered characteristics (20).

Confocal microscopy revealed a plasma membrane localization of the I130N-V2R and intracellular vesicles could not be identified (Fig. 2). This observation was similar to the cellular distribution of the F229V mutant (11) and it can be explained by the lack of basal β-arrestin binding of the I130N-V2R. However, the measurement of the plasma membrane

density of the mutant with flow cytometry showed reduced cell surface presence of the I130N-V2R (Fig 4A).

We also investigated the internalization properties of the mutant receptor (18, 21). The agonist stimulation induced a decrease in the BRET ratio, which indicates rapid internalization of the I130N-V2R (Fig 4C). Consistently with the flow cytometry measurements, the lower basal BRET ratio of I130N-V2R-Sluc with MP-YFP reflects the decreased plasma membrane localization, which could be further reduced upon AVP stimulus. Tolvaptan resulted in a slow increase of the BRET ratio between the I130N-V2R-Sluc and MP-YFP, but not in the cells expressing the wild type receptor (Fig 4B). Therefore, the constitutive activity of the I130N-V2R not only affects cAMP production, but also leads to internalization of the receptor, which could be blocked with inverse agonist tolvaptan. In contrast to the R137C/L mutants, I130N-V2R does not bind β-arrestin in the absence of agonist, but shows constitutive internalization, which can be inhibited with tolvaptan. This later observation suggests that the I130N mutation leads to different conformation from F229V mutation. Carpentier et al. concluded, that F229V mutation does not increase constitutive internalization of the receptor, although only receptor/β-arrestin and β-arrestin/AP2 interaction were measured with dominant negative dynamin or agonist treatment, and it was not shown whether the inverse agonists could affect the cell surface expression of the mutant (11). The dissimilarity in the agonist induced and constitutive internalization observed in this study in case of I130N-V2R is not unique among GPCRs, since β-arrestin-dependent, agonist-induced endocytosis and β-arrestin-independent constitutive internalization was introduced earlier (22-24). It is also notable, that basal internalization is not obviously a consequence of constitutive activity (25).

We examined the role of dynamin in the basal endocytosis to investigate the β-arrestin independent constitutive internalization. The expression of dominant-negative dynamin

resulted in increased plasma membrane localization I130N-V2R (Fig. 5B). Moreover, the effect of tolvaptan on constitutive internalization was less dramatic, compared to cells expressing wild-type dynamin. These data suggest that although basal endocytosis is β-arrestin-independent, it involves dynamin. Dominant-negative dynamin was shown to increase cell surface expression and β-arrestin/AP2 interaction of R137C/L receptors, which raises the possibility that the mutant receptors were trapped in the plasma membrane and accumulated in receptor-β-arrestin-AP2 complex (8). In contrast, F229V-V2R did not show increased β-arrestin/AP2 interaction in the case of co-expression of dominant-negative dynamin. This result was consistent with the absence of basal β-arrestin binding. The cell surface expression of the F229V in the presence of dominant-negative dynamin was not shown in this study (11). The internalization properties of I130N-V2R in the absence of agonist are not without example among the GPCRs. As it was described earlier, endocytotic pathways appear to function with plasticity and there is β-arrestin-independent but dynamin-dependent internalization mechanisms (26-29).

In this study, we identified and characterized a new gain-of-function mutation of the V2R, which leads to NSIAD. The mutation leads to biased receptor conformation (Fig. 6). The I130N mutation was shown to lead to increased intracellular cAMP concentration. Since the constitutive internalization of I130N-V2R was dynamin-dependent but β-arrestin-independent, the G-protein dependent pathway can be selectively activated in this mutant receptor. Inhibition of the basal internalization resulted in an increased cell surface density. Based on our findings, tolvaptan could be used for treatment of hyponatremia and its consequences such as seizures in patients with NSIAD and carrying I130N-V2R mutation.

Materials and methods

Mutation analysis in the AVPR2 gene

Family history, clinical and laboratory data and signed informed consent were obtained from the index patient and his relatives. Mutation analysis in the *AVPR2* gene was performed via PCR and Sanger sequencing of the entire coding region of the gene and flanking intron-exon boundaries. PCR primer sequences were based on those previously published by Chen et al. (30). The database sequence NM000054 (transcript ENST337474) was used as reference sequence for *AVPR2*. Prediction of mutation disease-causing status was performed using the mutation taster algorithm (www.mutationtaster.org).

Molecular biology

Details of generation of the molecular biological constructs were described previously (16). Standard site-directed mutagenesis techniques were used to perform mutagenesis in order to generate I130N receptor constructs. In order to avoid incidental mutations, after verifying the mutations with dideoxy sequencing, the mutated fragment was exchanged between the wild type and mutated portion with suitable restriction sites. Construction of Epac-BRET was described previously (16). The cDNAs of the HA epitope-tagged wild-type and K44A mutant dynamins were subcloned into pcDNA3 vector, as previously described (31). The cDNA of C terminus of mRFP was fused to a cDNA of a nuclear localization signal [NLS; (DPKKKRKV)3] with a linker (SGLRSRAQASNSRV) in a C1 plasmid.

Cell culture and transfection

Cell culture protocols and transfection of cells in 96-well plates were described previously (16). Briefly, the DNA amounts were either 0.25 μg receptor containing construct/well and 0.25 μg BRET partner containing construct/well or in the case of co-transfection with three constructs of 0.2 μg receptor containing construct/well, 0.2 μg BRET partner containing construct/well and 0.2 μg untagged construct/well. The amount of Lipofectamine 2000 was 0.5 μl/well.

BRET measurements

BRET measurements were performed as described previously (16). We used either a *Renilla* luciferase-fused receptor as the energy donor and an eYFP-tagged protein as the acceptor or we used intramolecular BRET probe (cAMP measuring Epac-BRET). Dose-response sigmoidal curve was generated using non-linear regression by GraphPad Prism software. The statistical analysis was carried out with two way ANOVA and Bonferroni post hoc test.

Confocal microscopy

The cells plated on polylysine-pretreated glass coverslips (3×10^5 cells/35-mm dish) and were transiently transfected with the HA-tagged receptor constructs (1 μg of receptor/well; the amount of Lipofectamine 2000 was 4 μl/well.) and NLS-mRFP (0,125 μg/well). After 24 hours, the cells were washed 3 times with ice cold 1% bovine serum albumin–containing modified Krebs-Ringer buffer (21) solution. For immunostaining, the anti-HA-Alexa 488 mouse monoclonal antibodies were diluted to 1:250 and the cells were incubated for 30 minutes on 4°C. Cells were washed and analyzed in ice-cold modified Krebs-Ringer buffer. For the co-localization studies, cells transiently transfected with the mVenus-tagged receptor constructs (1 μg of receptor/well; the amount of Lipofectamine 2000 was 4 μl/well.), NLS-mRFP and MP-Cerulean (0,125 μg/well). The localization and distribution of the targeted probes were analyzed using a Zeiss LSM710 confocal laser-scanning microscope.

Flow cytometry

Cells were plated on glass coverslips (3×10^5 cells/35-mm dish) and transiently transfected with the HA-tagged receptor constructs or pcDNA3.1. The cells were detached by Versene reagent treatment and were centrifuged. The cells were suspended in ice-cold PBS and

centrifuged at 4 ^{o}C. The cell pellets were suspended and incubated with diluted (1:100) anti-HA-Alexa488 mouse monoclonal antibodies for 40 minutes on 4 ^{o}C. After the labeling period the cells were washed in ice-cold PBS. Flow cytometry measurements were performed with Beckman-Coulter SC. After measuring the fluorescent intensity of the cells, G_{mean} was calculated using WinMDI v2.9 (http://facs.scripps.edu). For the relative fluorescent intensity the background (pcDNA3.1) was subtracted and the data were normalized for the wild type receptor. Statistical analysis was carried out using two-way ANOVA.

Disclosures

The authors declare that there is no conflict of interest that could be perceived as prejudicing the impartiality of the research reported.

Acknowledgements

This work was supported by Hungarian Ministry of National Resources (grant OTKA 100883).

References

1. Schoneberg T, Schulz A, Biebermann H*, et al.* Mutant G-protein-coupled receptors as a cause of human diseases. *Pharmacology & therapeutics* 2004; 104**:** 173-206.

2. Feldman BJ, Rosenthal SM, Vargas GA*, et al.* Nephrogenic syndrome of inappropriate antidiuresis. *The New England journal of medicine* 2005; 352**:** 1884-1890.

3. Moeller HB, Rittig S, Fenton RA. Nephrogenic diabetes insipidus: essential insights into the molecular background and potential therapies for treatment. *Endocrine reviews* 2013; 34**:** 278-301.

4. Ligeti E, Csepanyi-Komi R, Hunyady L. Physiological mechanisms of signal termination in biological systems. *Acta physiologica (Oxford, England)* 2012; 204**:** 469-478.

5. Barak LS, Oakley RH, Laporte SA*, et al.* Constitutive arrestin-mediated desensitization of a human vasopressin receptor mutant associated with nephrogenic diabetes insipidus. *Proceedings of the National Academy of Sciences of the United States of America* 2001; 98**:** 93-98.

6. Spanakis E, Milord E, Gragnoli C. AVPR2 variants and mutations in nephrogenic diabetes insipidus: review and missense mutation significance. *Journal of cellular physiology* 2008; 217**:** 605-617.

7. Kocan M, See HB, Sampaio NG*, et al.* Agonist-independent interactions between beta-arrestins and mutant vasopressin type II receptors associated with nephrogenic syndrome of inappropriate antidiuresis. *Molecular endocrinology* 2009; 23**:** 559-571.

8. Rochdi MD, Vargas GA, Carpentier E*, et al.* Functional characterization of vasopressin type 2 receptor substitutions (R137H/C/L) leading to nephrogenic diabetes insipidus and nephrogenic syndrome of inappropriate antidiuresis: implications for treatments. *Molecular pharmacology* 2010; 77**:** 836-845.

9. Miyazaki T, Yamamura Y, Onogawa T*, et al.* Therapeutic effects of tolvaptan, a potent, selective nonpeptide vasopressin V2 receptor antagonist, in rats with acute and chronic severe hyponatremia. *Endocrinology* 2005; 146**:** 3037-3043.

10. Decaux G, Vandergheynst F, Bouko Y*, et al.* Nephrogenic syndrome of inappropriate antidiuresis in adults: high phenotypic variability in men and women from a large pedigree. *J Am Soc Nephrol* 2007; 18**:** 606-612.

11. Carpentier E, Greenbaum LA, Rochdi D*, et al.* Identification and characterization of an activating F229V substitution in the V2 vasopressin receptor in an infant with NSIAD. *J Am Soc Nephrol* 2012; 23**:** 1635-1640.

12. Schulz A, Sangkuhl K, Lennert T*, et al.* Aminoglycoside pretreatment partially restores the function of truncated V(2) vasopressin receptors found in patients with nephrogenic diabetes insipidus. *The Journal of clinical endocrinology and metabolism* 2002; 87**:** 5247-5257.

13. Armstrong SP, Seeber RM, Ayoub MA*, et al.* Characterization of Three Vasopressin Receptor 2 Variants: An Apparent Polymorphism (V266A) and Two Loss-of-Function Mutations (R181C and M311V). *PloS one* 2013; 8**:** e65885.

14. Cho YH, Gitelman S, Rosenthal S*, et al.* Long-term outcomes in a family with nephrogenic syndrome of inappropriate antidiuresis. *International journal of pediatric endocrinology* 2009; 2009**:** 431527.

15. Levtchenko EN, Monnens LA. Nephrogenic syndrome of inappropriate antidiuresis. *Nephrology, dialysis, transplantation : official publication of the European Dialysis and Transplant Association - European Renal Association* 2010; 25**:** 2839-2843.

16. Erdelyi LS, Balla A, Patocs A*, et al.* Altered agonist sensitivity of a mutant v2 receptor suggests a novel therapeutic strategy for nephrogenic diabetes insipidus. *Molecular endocrinology* 2014; 28**:** 634-643.

17. Takahashi K, Makita N, Manaka K*, et al.* V2 vasopressin receptor (V2R) mutations in partial nephrogenic diabetes insipidus highlight protean agonism of V2R antagonists. *The Journal of biological chemistry* 287**:** 2099-2106.

18. Toth DJ, Toth JT, Gulyas G*, et al.* Acute depletion of plasma membrane phosphatidylinositol 4,5-bisphosphate impairs specific steps in endocytosis of the G-protein-coupled receptor. *Journal of cell science* 2012; 125**:** 2185-2197.

19. Varnai P, Toth B, Toth DJ*, et al.* Visualization and manipulation of plasma membrane-endoplasmic reticulum contact sites indicates the presence of additional molecular components within the STIM1-Orai1 Complex. *The Journal of biological chemistry* 2007; 282**:** 29678-29690.

20. Wei H, Ahn S, Shenoy SK*, et al.* Independent beta-arrestin 2 and G protein-mediated pathways for angiotensin II activation of extracellular signal-regulated kinases 1 and 2. *Proceedings of the National Academy of Sciences of the United States of America* 2003; 100**:** 10782-10787.

21. Balla A, Toth DJ, Soltesz-Katona E*, et al.* Mapping of the localization of type 1 angiotensin receptor in membrane microdomains using bioluminescence resonance energy transfer-based sensors. *The Journal of biological chemistry* 2012; 287**:** 9090-9099.

22. Dale LB, Bhattacharya M, Seachrist JL*, et al.* Agonist-stimulated and tonic internalization of metabotropic glutamate receptor 1a in human embryonic kidney 293 cells: agonist-stimulated endocytosis is beta-arrestin1 isoform-specific. *Molecular pharmacology* 2001; 60**:** 1243-1253.

23. Holliday ND, Lam CW, Tough IR*, et al.* Role of the C terminus in neuropeptide Y Y1 receptor desensitization and internalization. *Molecular pharmacology* 2005; 67**:** 655-664.

24. Parent JL, Labrecque P, Driss Rochdi M*, et al.* Role of the differentially spliced carboxyl terminus in thromboxane A2 receptor trafficking: identification of a distinct motif for tonic internalization. *The Journal of biological chemistry* 2001; 276**:** 7079-7085.

25. Gyombolai P, Boros E, Hunyady L*, et al.* Differential beta-arrestin2 requirements for constitutive and agonist-induced internalization of the CB1 cannabinoid receptor. *Molecular and cellular endocrinology* 2013; 372**:** 116-127.

26. Bhatnagar A, Willins DL, Gray JA*, et al.* The dynamin-dependent, arrestin-independent internalization of 5-hydroxytryptamine 2A (5-HT2A) serotonin receptors reveals differential sorting of arrestins and 5-HT2A receptors during endocytosis. *The Journal of biological chemistry* 2001; 276**:** 8269-8277.

27. Claing A, Laporte SA, Caron MG*, et al.* Endocytosis of G protein-coupled receptors: roles of G protein-coupled receptor kinases and beta-arrestin proteins. *Progress in neurobiology* 2002; 66**:** 61-79.

28. Okamoto Y, Ninomiya H, Miwa S*, et al.* Cholesterol oxidation switches the internalization pathway of endothelin receptor type A from caveolae to clathrin-coated pits in Chinese hamster ovary cells. *The Journal of biological chemistry* 2000; 275**:** 6439-6446.

29. Smyth EM, Austin SC, Reilly MP*, et al.* Internalization and sequestration of the human prostacyclin receptor. *The Journal of biological chemistry* 2000; 275**:** 32037-32045.

30. Chen CH, Chen WY, Liu HL*, et al.* Identification of mutations in the arginine vasopressin receptor 2 gene causing nephrogenic diabetes insipidus in Chinese patients. *Journal of human genetics* 2002; 47**:** 66-73.

31. Szaszak M, Gaborik Z, Turu G*, et al.* Role of the proline-rich domain of dynamin-2 and its interactions with Src homology 3 domains during endocytosis of the AT1 angiotensin receptor. *The Journal of biological chemistry* 2002; 277**:** 21650-21656.

Titles and legends

Fig. 1

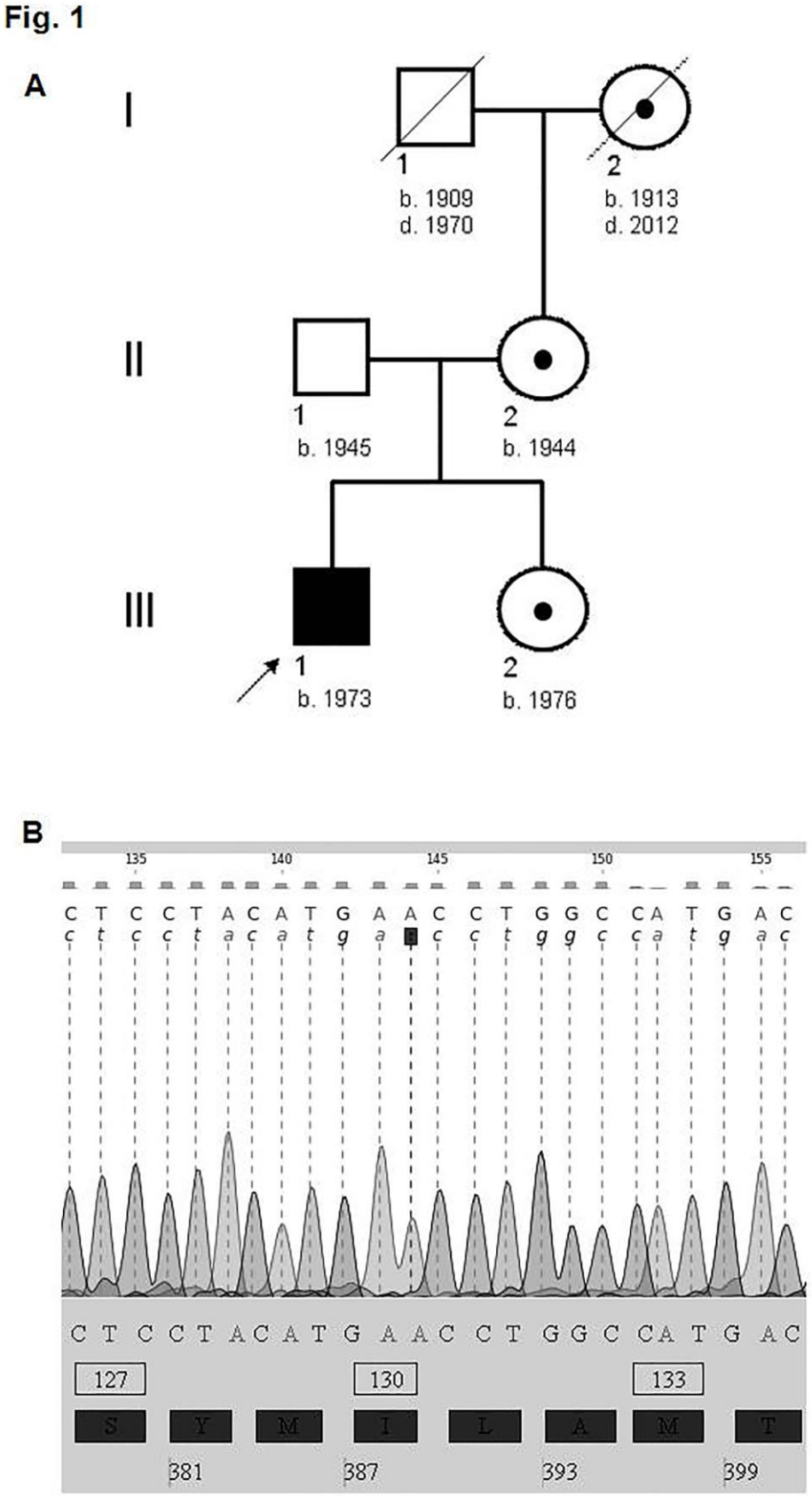

Fig. 1 A: Pedigree of the family with X-linked congenital nephrogenic syndrome of inappropriate diuresis (NSIAD) due to a novel mutation. Arrow indicates the index patient. The hemizygous male is represented by a solid square. Heterozygous females are represented by open circles with a central dot. An open square indicates an unaffected male, genotyped wild type. Year of birth (b.) or death (d.) is placed below the symbol. A slash through the symbol indicates a deceased individual. Roman numerals denote the generation. Arabic numerals denote the individuals in each generation. **B: Mutational analysis in *AVPR2*.** Mutation analysis by direct DNA sequencing of PCR fragments from the proband and his family revealed a novel missense mutation p.Ile130Asn, c.389T>A in exon 2 of the *AVPR2* gene. The proband showed a hemizygous mutation. His mother (II.2), his grandmother (I.2) and the proband´s sister (III.2) were heterozygous for the p.Ile130Asn mutation whereby their carrier status was confirmed.

Fig. 2.

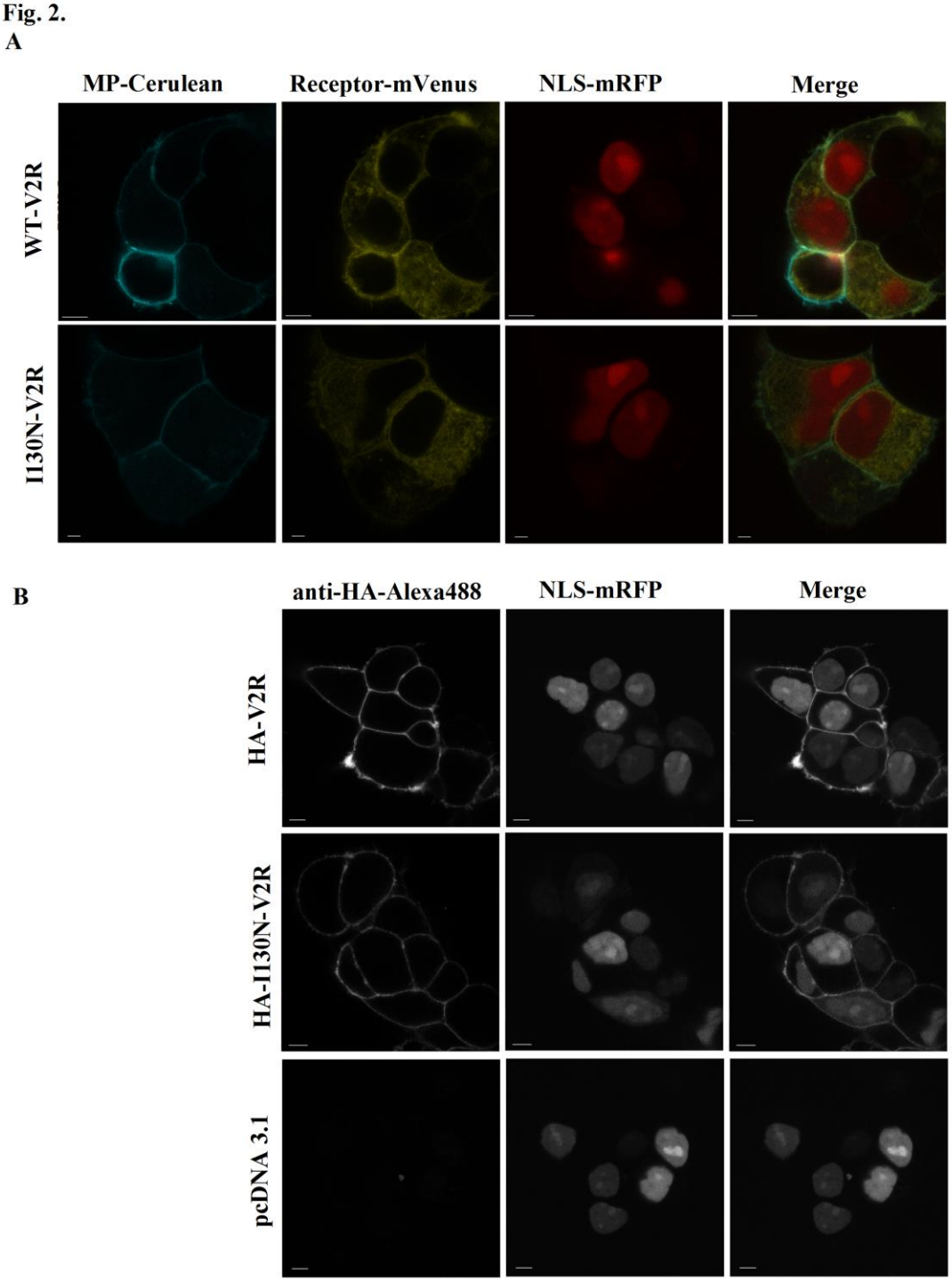

Figure 2: Examination of the plasma membrane and intracellular expression of the I130N-V2R.

(A) Confocal microscopy analysis of HEK293 cells transiently expressing MP-Cerulean, NLS-mRFP and either mVenus-tagged WT-V2R or mVenus-tagged I130N-V2R. (B) Confocal microscopy analysis of HEK293 cells transiently expressing NLS-mRFP and either HA-tagged V2R or HA-tagged I130N-V2R. Immunofluorescent staining was implemented with anti-HA-Alexa488 mouse monoclonal antibodies. Scale bars represent 5 μm.

Fig. 3

A

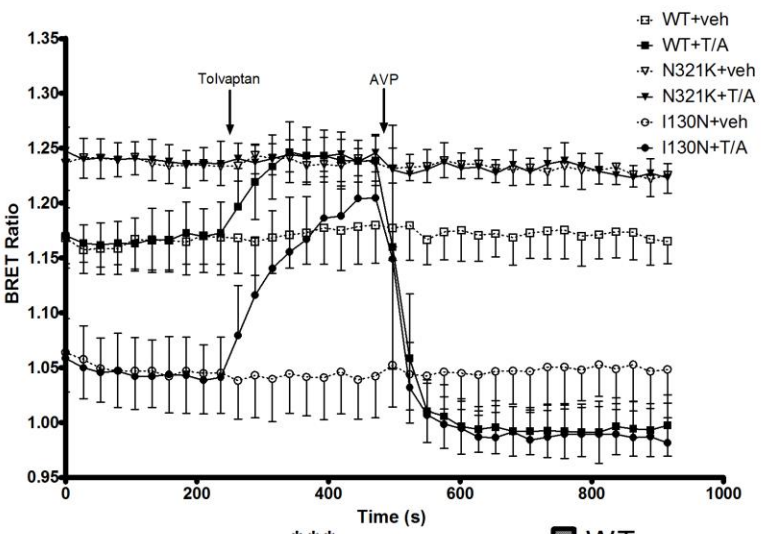
WT+veh
WT+T/A
N321K+veh
N321K+T/A
I130N+veh
I130N+T/A
Tolvaptan
AVP
BRET Ratio
Time (s)

B

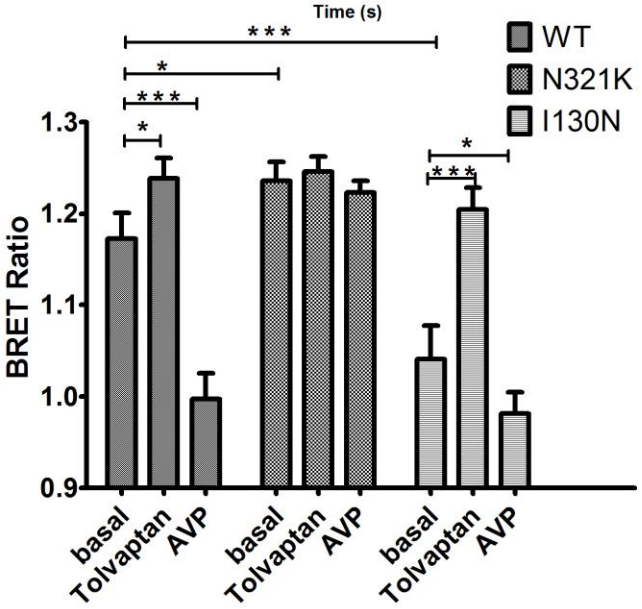
WT
N321K
I130N
BRET Ratio
basal
Tolvaptan
AVP

C

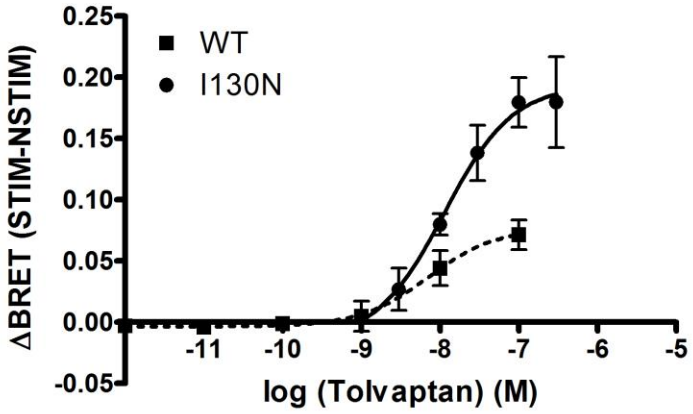
WT
I130N
ΔBRET (STIM-NSTIM)
log (Tolvaptan) (M)

Figure 3: Measurement of the basal cAMP signal and the cAMP production after tolvaptan and AVP stimuli. HEK293 cells were transiently transfected with WT-V2R (square), I130N-V2R (circle) or N321K-V2R (triangle) and the Epac-BRET sensor. After 24 h, the BRET measurements were implemented. Mean values ± SD are shown (n = 3, * $p < 0.05$, *** $p<0.001$). (A) The cells were stimulated sequentially with 100 nM tolvaptan and 1 µM AVP at the indicated time (filled marks). (B) The BRET ratios represent the last points before the next stimulus from Fig. 4A. (C) Dose response curve of wild type (square) and I130N-V2R (circle) upon tolvaptan treatment. The effect of the inverse agonist on the WT-V2R and N321K-V2R expressing HEK293 cells was calculated as the BRET ratio difference between the ligand (stim) and the vehicle (nstim) treated cells at the first time points after the treatment.

Fig. 4

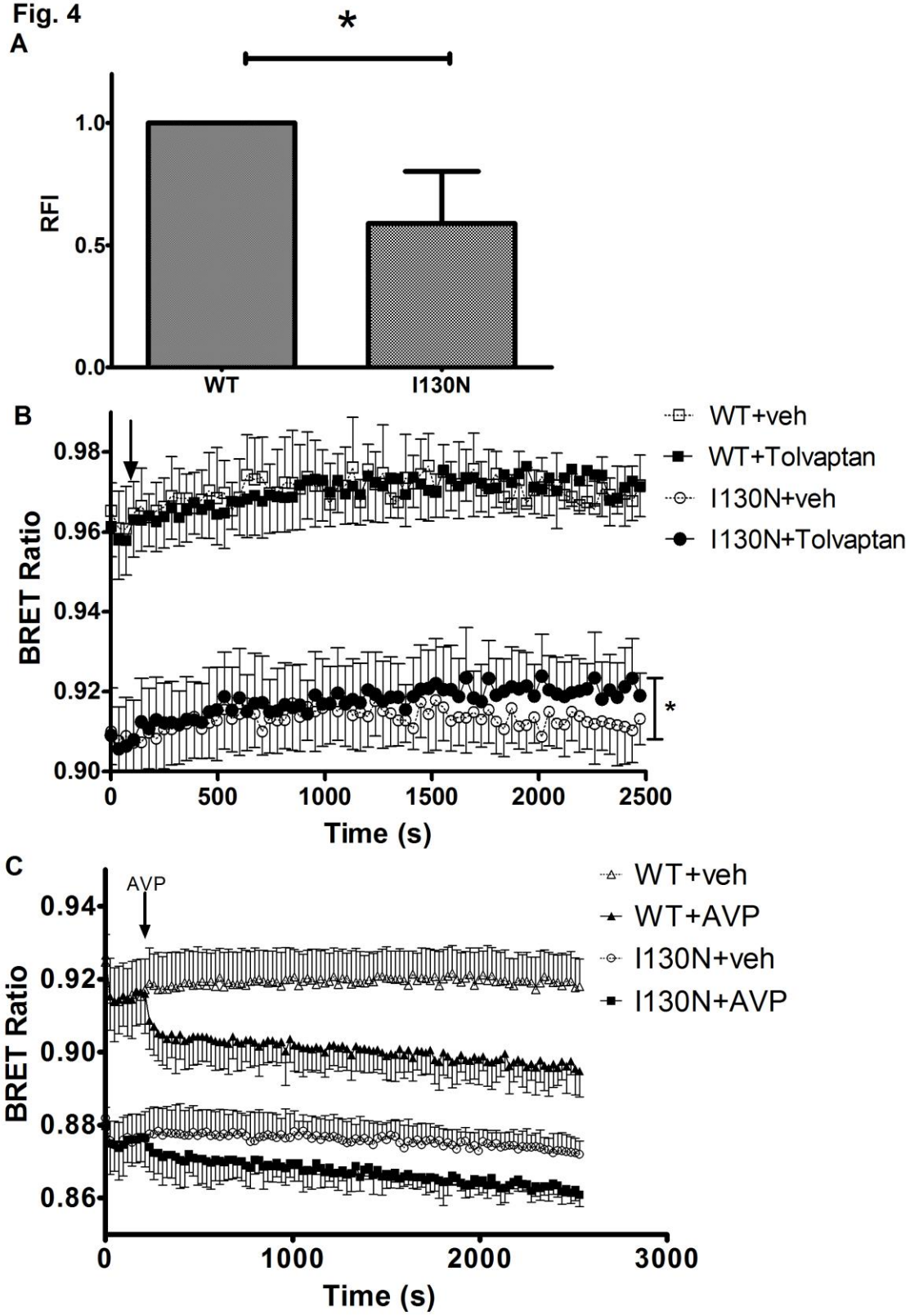
A
*
1.0
0.5
0.0
RFI
WT
I130N
B
WT+veh
WT+Tolvaptan
I130N+veh
I130N+Tolvaptan
0.98
0.96
0.94
0.92
0.90
BRET Ratio
*
0
500
1000
1500
2000
2500
Time (s)
C
AVP
WT+veh
WT+AVP
I130N+veh
I130N+AVP
0.94
0.92
0.90
0.88
0.86
BRET Ratio
0
1000
2000
3000
Time (s)

Figure 4: Measurement of cells surface expression and internalization properties of I130N-V2R. (A) Cell surface expression values of the V2Rs were quantified after labeling with anti-HA-Alexa488 mouse monoclonal antibodies using flow cytometry determinations. After measuring the fluorescent intensity of the cells, G_{mean} was calculated. For the relative fluorescent intensity the background (pcDNA3.1) was subtracted and the data were normalized for the wild type receptor. Mean values ± SD are shown ($n = 4$, $p<0.05$). (B and C) HEK293 cells were transiently transfected with the plasmids of the indicated BRET partners (WT-V2R-Sluc or I130N-V2R-Sluc and MP-YFP) and after 24h BRET measurements were implemented. Mean values ± SD are shown ($n = 3$, $p<0.05$). (B) Cells were exposed to 100 nM tolvaptan (filled marks) or vehicle (open symbols) at the indicated time. (C) Cells were exposed to 1 μM AVP (filled marks) or vehicle (open symbols) at the indicated time.

Fig. 5

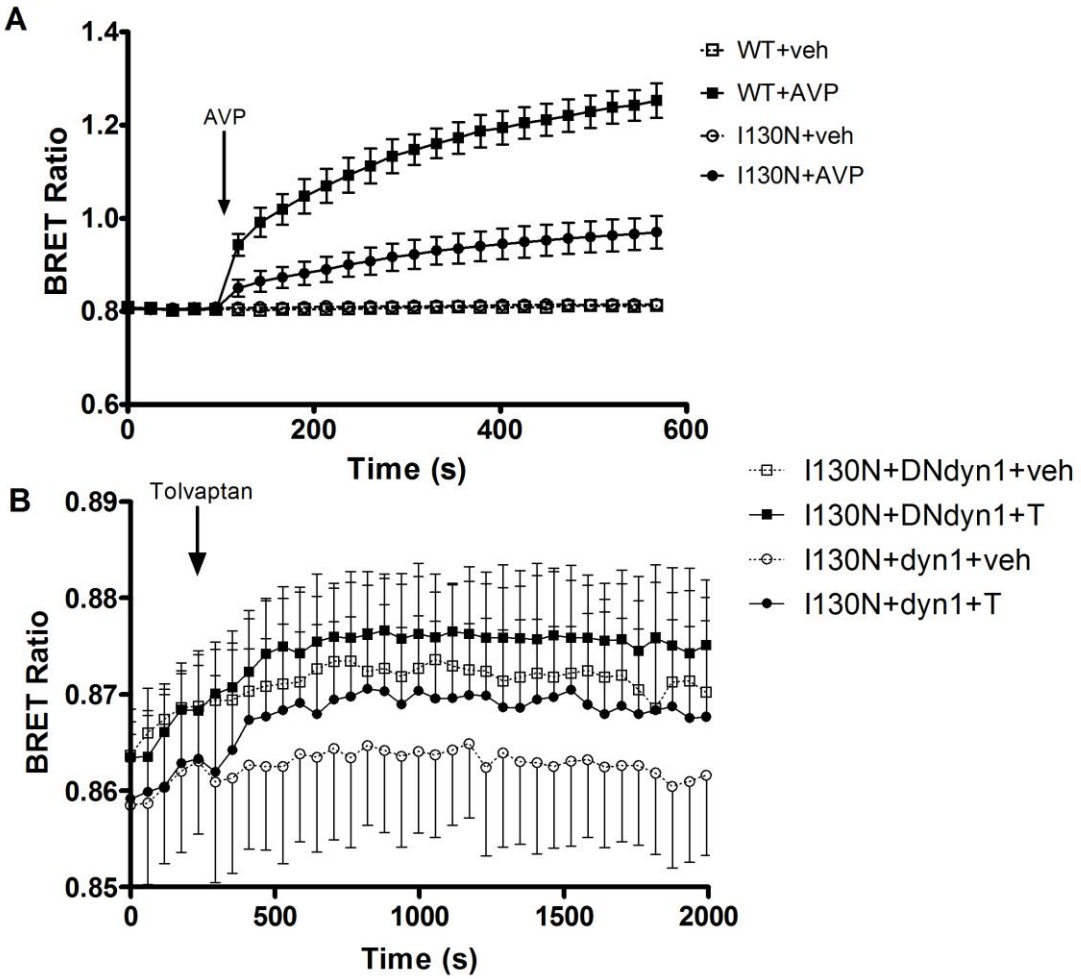
A
BRET Ratio
1.4
1.2
1.0
0.8
0.6
AVP
0
200
400
600
Time (s)
WT+veh
WT+AVP
I130N+veh
I130N+AVP
B
BRET Ratio
0.89
0.88
0.87
0.86
0.85
Tolvaptan
0
500
1000
1500
2000
Time (s)
I130N+DNdyn1+veh
I130N+DNdyn1+T
I130N+dyn1+veh
I130N+dyn1+T

Figure 5: Investigation of internalization properties of I130N-V2R. (A) Examination of β-arrestin binding properties of I130N-V2R. β-arrestin binding was measured with the transfection of wild type (square)- or I130N-V2R-mVenus (circle) and β-arrestin-Rluc plasmids. Cells were exposed either to 1μM AVP (filled symbols) or vehicle (open symbols) at the indicated time point. Mean values ± SD are shown (n = 3). (**B)** Examination of the effect of dominant negative dynamin on the internalization of I130N-V2R. HEK293 cells were transiently transfected with the plasmids of the indicated BRET partners (I130N-V2R-Sluc and MP-YFP) and dynamin constructs (wild type or dominant negative) and after 24h BRET measurements were implemented. Cells were exposed to 100 nM tolvaptan (filled marks) or vehicle (open symbols) at the indicated time. Mean values ± S.E. are shown (n = 3).

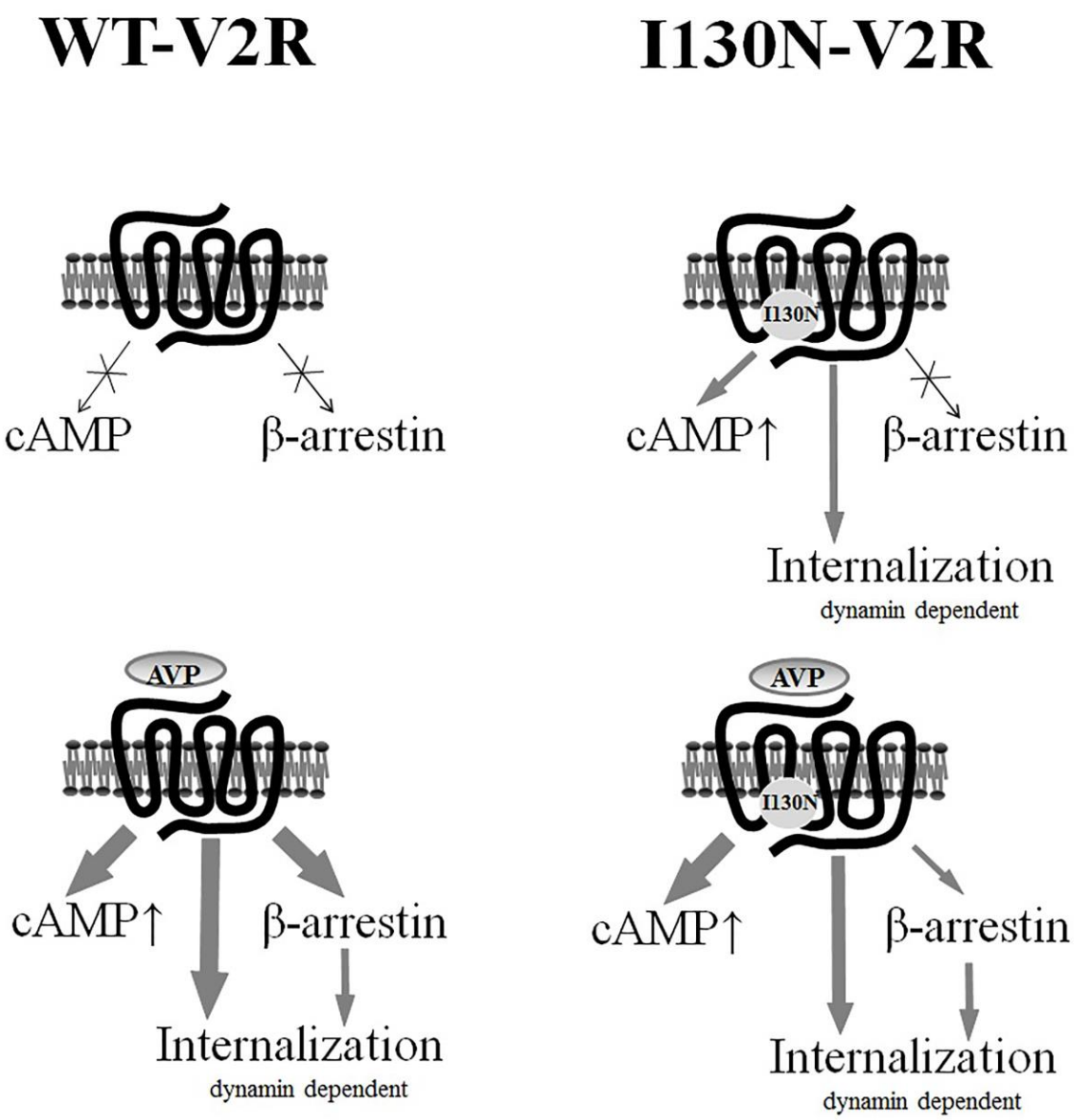

Figure 6: Schematic illustration of the consequences of I130N missense mutation in the V2R. Thickness of the arrows represent the magnitude of cAMP signal, internalization and β-arrestin binding.

Table 1.

Characteristic	Patient data	Normal values
Age at presentation	28	-
Clinically significant findings	palpitations	-
Blood pressure (mm HG)		
Systolic	120	< 140
diastolic	80	< 90
Serum and plasma analysis		
Sodium (mmol/liter)	121	136-145
Potassium (mmol/liter)	4.4	3.5-4.8
Creatinine (mg/dl)	0.7	0.7-1.2
Glomerular filtration rate (Mmol / min)	136	60 - 160
Urea nitrogen (mg/dl)	16.9	16.6 – 48.5
ACTH (ng/l)	10.8	4.7-48.8
Cortisol (ng/ml)	59.5	23-194
Aldosteron (ng/l)	56	40 - 310
Renin (ng/ml/h)	1.73	0.2 - 2.8
Serum Osmolality (mOsm/kg)	205	280 - 300
AVP (ng /l)	< 0.6	0 – 7.8
Urine analysis		
Urine Spezific weight (g/l)	1020	1000 - 1030

Sodium excretion (mmol/24h)	300.6	40 - 220
Urine Osmolality (mOsm/kg)	652	50 - 1200

Table 1: Clinical characteristics of the index patient

Table 2.

Patient number	Age (years)	Serum sodium (mmol/l)	A*AVPR2* gene
I.2	95	123	c.389T>A
II.1	62	140	wt
II.2	63	130	c.389T>A
III.1	34	121	c.389T>A
III.2	31	139	c.389T>A

Table 2: Clinical and laboratory characteristics of the family members

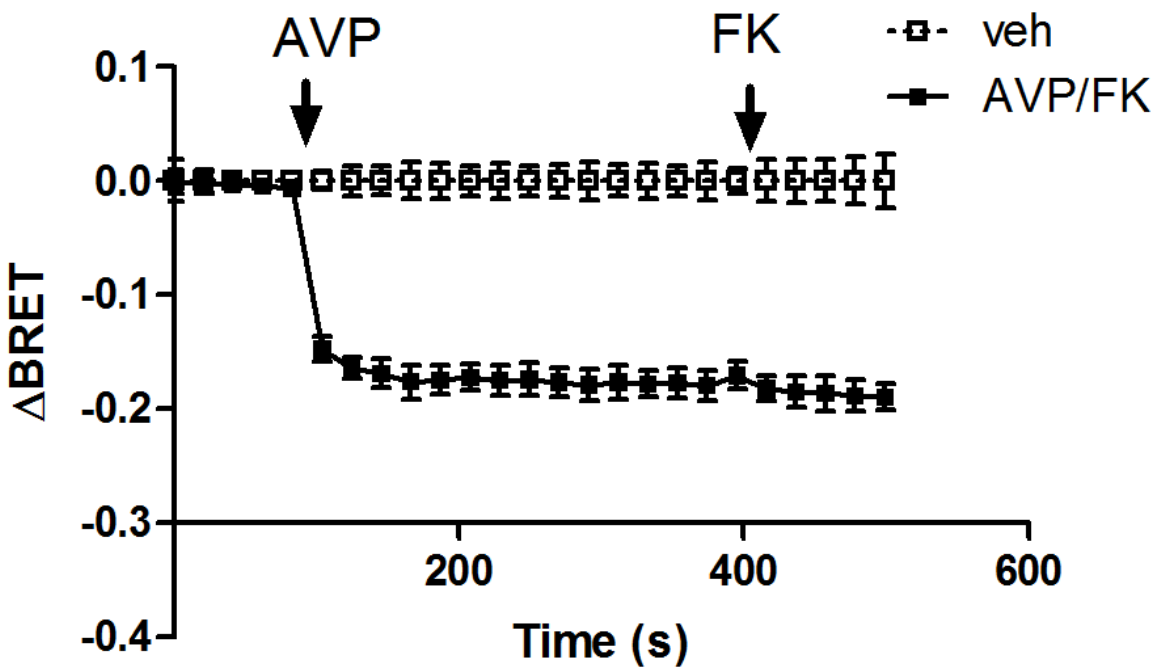

Supplementary figure 1: Measurement of the cAMP production after AVP and forskolin stimulations. HEK293 cells were transiently transfected with WT-V2R and the Epac-BRET sensor. After 24 h, the BRET measurements were implemented. Mean values ± S.E. are shown (n = 3). The cells were stimulated sequentially with 1 µM AVP and 10 µM forskolin at the indicated time (filled marks).

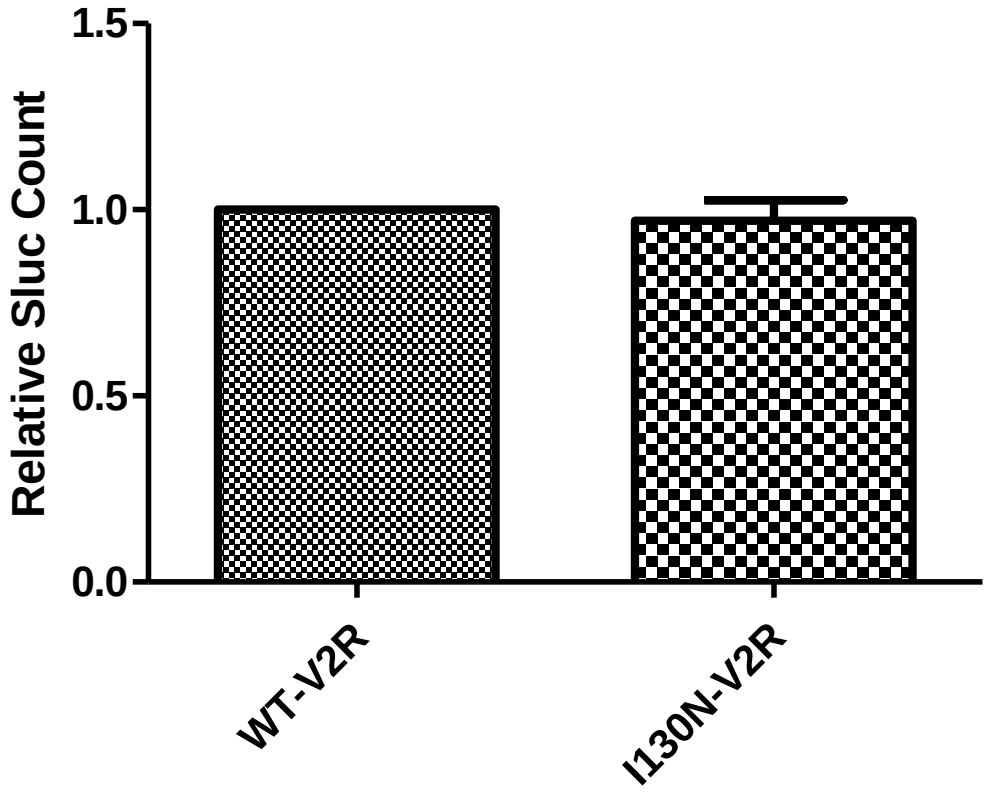

Supplementary figure 2: Relative Sluc counts of the WT-V2R and I130N-V2R measured after cell permeable substrate coelenterazine treatment. The Sluc counts of the tagged receptors were obtained from the BRET experiment in Fig 4B. The averages of the counts were calculated from the non-stimulated Sluc counts (before tolvaptan or vehicle stimulation) of the wells in the first two cycles. The averages were normalized in each experiment the WT-V2R. Mean values ± S.E. are shown (n = 3).

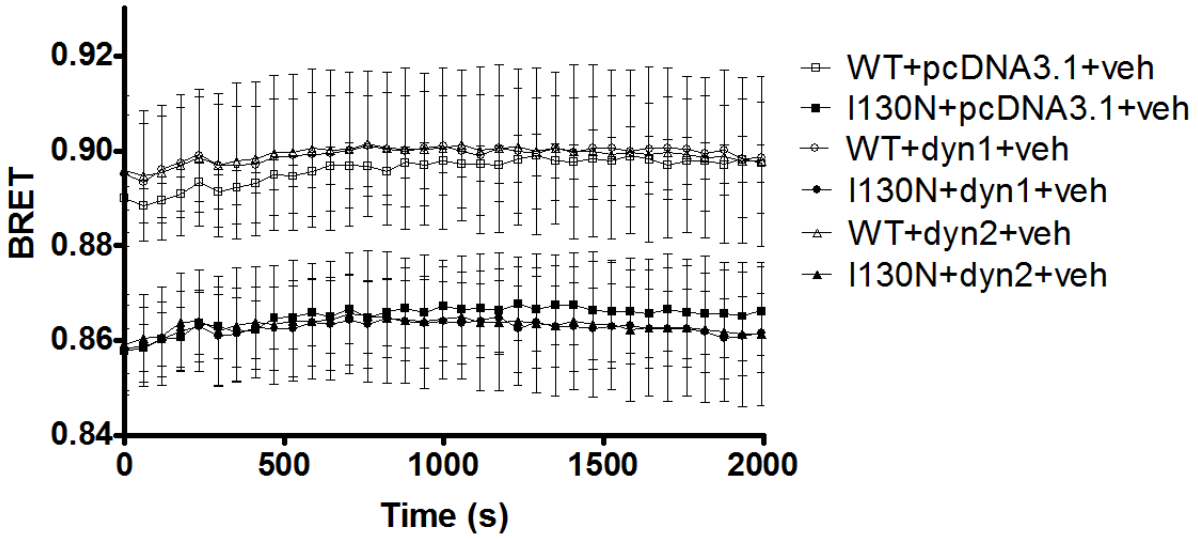

Supplementary figure 3: Control measurements for the examination of the effect of dominant negative dynamin on the internalization of I130N-V2R. HEK293 cells were transiently transfected with the plasmids of the indicated BRET partners (I130N-V2R-Sluc or WT-V2R-Sluc and MP-YFP) and wild type dynamin constructs (dynamin1 or -2) or empty pcDNA3.1 vector and after 24h BRET measurements were implemented. Mean values ± S.E. are shown (n = 3).